Mixing state of aerosols and direct observation of carbonaceous and marine coatings on African dust by individual particle analysis

Karine Deboudt,[1,2] Pascal Flament,[1,2] Marie Choël,[1,3] Alexandre Gloter,[4] Sophie Sobanska,[1,3] and Christian Colliex[4]

Received 22 January 2010; revised 26 July 2010; accepted 27 August 2010; published 18 December 2010.

[1] The mixing state of aerosols collected at M'Bour, Senegal, during the Special Observing Period conducted in January–February 2006 (SOP-0) of the African Monsoon Multidisciplinary Analysis project (AMMA), was studied by individual particle analysis. The sampling location on the Atlantic coast is particularly adapted for studying the mixing state of tropospheric aerosols since it is (1) located on the path of Saharan dust plumes transported westward over the northern tropical Atlantic, (2) influenced by biomass burning events particularly frequent from December to March, and (3) strongly influenced by anthropogenic emissions from polluted African cities. Particle size, morphology, and chemical composition were determined for 12,672 particles using scanning electron microscopy (automated SEM-EDX). Complementary analyses were performed using transmission electron microscopy combined with electron energy loss spectrometry (TEM-EELS) and Raman microspectrometry. Mineral dust and carbonaceous and marine compounds were predominantly found externally mixed, i.e., not present together in the same particles. Binary internally mixed particles, i.e., dust/carbonaceous, carbonaceous/marine, and dust/marine mixtures, accounted for a significant fraction of analyzed particles (from 10.5% to 46.5%). Western Sahara was identified as the main source of mineral dust. Two major types of carbonaceous particles were identified: "tar balls" probably coming from biomass burning emissions and soot from anthropogenic emissions. Regarding binary internally mixed particles, marine and carbonaceous compounds generally formed a coating on mineral dust particles. The carbonaceous coating observed at the particle scale on African dust was evidenced by the combined use of elemental and molecular microanalysis techniques, with the identification of an amorphous rather than crystallized carbon structure.

Citation: Deboudt, K., P. Flament, M. Choël, A. Gloter, S. Sobanska, and C. Colliex (2010), Mixing state of aerosols and direct observation of carbonaceous and marine coatings on African dust by individual particle analysis, *J. Geophys. Res.*, *115*, D24207, doi:10.1029/2010JD013921.

1. Introduction

[2] The West African troposphere is periodically perturbed by Saharan dust events, occurring mainly during the dry season (November to April). These events are able to transport mineral dust particles over long distances and may impact Europe. Nevertheless, in an overall description of the atmospheric particulate matter in the Sahelian zone, other sources have to be considered. During the dry season, biomass burning aerosols and associated gaseous compounds originating from savanna fires are abundant (mostly from December to March) [*Liousse et al.*, 1996] and their interaction with mineral dust can be significant. The particulate and gaseous emissions from African cities have also to be considered. Because of the absence of emission reduction laws, African cities significantly contribute to global and regional atmospheric pollution [*Hopkins et al.*, 2009]. During the westward transport of African air masses over the northern tropical Atlantic in the dry season, atmospheric pollutants from these different sources have a high probability to evolve into internal mixtures. These complex heterogeneous mixtures have a significant impact on radiative properties of aerosols not only on a regional but also on a global scale. The role of black carbon (BC) in global climate change is of prime importance since BC is a light-absorbing carbonaceous component of submicron aerosols. BC optical properties are strongly dependent on its chemical (e.g., composition) and physical (e.g., size, morphology) properties and notably on its mixing state [*Jacobson*, 2001].

[1]Université Lille Nord de France, Lille, France.
[2]Laboratoire de Physico-Chimie de l'Atmosphere, UMR CNRS 8101, Université du Littoral Côte d'Opale, Dunkerque, France.
[3]Laboratoire de Spectrochimie InfraRouge et Raman, UMR CNRS 8516, Université des Sciences et Technologies de Lille, Villeneuve d'Ascq, France.
[4]Laboratoire de Physique des Solides, UMR CNRS 8502, Université de Paris-Sud 11, Orsay, France.

0148-0227/10/2010JD013921

A good knowledge of the mixing state of aerosols is necessary to obtain a good closure in optical property measurements and to reduce large remaining uncertainties in the radiative forcing of aerosols.

[3] The Special Observing Period conducted during January–February 2006 (SOP-0) of the African Monsoon Multidisciplinary Analysis (AMMA) project was aimed at studying the dry phase of the monsoon cycle. One of the AMMA surface measurement stations was M'Bour, Senegal, on the Atlantic coast. It is particularly suitable for studying the mixing state of tropospheric aerosols since it is located on the pathway of desert dust plumes transported westward over the northern tropical Atlantic, and is also strongly influenced by emissions from regional anthropogenic activities. Aerosol size distribution and spectral absorption over M'Bour during the SOP-0 by *Derimian et al.* [2008] were found to be representative of the climatological state even if no major dust events occurred and the aerosol loading was 25% below the average values measured for the same period of previous years. Vertical profiles of aerosol extinction derived from LIDAR measurement suggested generally two layers: high-altitude transport (up to about 4 km) of predominantly biomass burning aerosols from forest fires to the south and east, and lower-altitude transport of essentially mineral dust [*Derimian et al.*, 2008]. This result was consistent with aircraft observations performed in the region during the same period [*Johnson et al.*, 2008; *Osborne et al.*, 2008]. These two layers (i.e., the upper air mass transporting mainly biomass burning aerosols and the lower air mass carrying essentially mineral dust) are not completely separated and mixing can occur at the interface [*Haywood et al.*, 2008].

[4] In this context, our study focuses on the scavenging of carbonaceous and marine compounds by African dust during the AMMA SOP-0 using single-particle analysis. Size, morphology and chemical composition of atmospheric particles can be obtained by analytical electron microscopy [*Choël et al.*, 2007; *Ebert et al.*, 2004; *Laskin and Cowin*, 2001; *Ro et al.*, 2005] and Raman microspectroscopy [*Batonneau et al.*, 2006; *Ivleva et al.*, 2007]. Transmission electron miscroscopy combined with electron energy loss spectrometry (TEM-EELS) is an accurate technique for low-Z element analysis especially when a good resolution is required [*Chen et al.*, 2005; *Mavrocordatos et al.*, 2004]. The mixing state of particles can be determined accurately for several size ranges, on condition that a large number of particles (typically a few thousands) are examined per sample. Moreover, to our knowledge, the internal mixing of African dust with carbonaceous compounds is rarely reported at the particle scale by scanning electron microscopy because an adapted substrate for aerosol collection is necessary to detect characteristic X-rays and accurately quantify both light (C, N, O) and heavy elements. In the present work, homemade boron substrates were employed [*Choël et al.*, 2005].

2. Sampling and Analytical Methodology

2.1. Sampling Location (AMMA SOP Station)

[5] Sampling campaigns were carried out during the "dry season" (SOP-0), from 2 February to 15 February 2006, south of M'Bour (14°23′38″N, 16°57′32″W), Senegal, at a ground-based station of the AMMA network. M'Bour is a coastal city of 180,000 inhabitants, located 90 km south of Dakar. During the dry season, the dominant winds in Senegal are the north to northeast maritime trade wind and the Harmattan, a continental wind which has a dominant east direction. Local meteorological conditions (temperature, relative humidity, wind speed, wind direction and pressure) were recorded automatically every 5 min. The sampling station, characterized by onshore synoptic flow (continental breeze), is located near the seashore. Transition to offshore flow (sea breeze) was regularly detected in the afternoon from the local wind direction. This sea breeze could increase the impact of local influences on atmospheric particulate matter compared to long-range transport, but this eventual impact is limited by sampling atmospheric aerosols just before its formation, i.e., each day for 1 h in the late morning (1145–1245 UTC).

2.2. Air Mass Trajectories

[6] To characterize the transport pathways and the potential aerosol source regions associated with the air masses sampled, 120 h synoptic trajectories were calculated with the hybrid single-particle lagrangian integrated trajectories (HYSPLIT) model [*Draxler and Hess*, 1998]. Meteorological data from the National Weather Service's National Center for Environmental Prediction (NCEP) FNL data set were used [*Stunder*, 1997]. Backward trajectories ending at the altitude of 500 m were calculated at the beginning and at the end of aerosol samplings. An ending point at 500 m of altitude should give a good approximation to the mean transport air masses since this altitude frequently lies near the center of the boundary layer and uncertainties because of local turbulence near the ground should be limited compared to a trajectory ending at the ground. To validate this ending position, ensembles of trajectories with slightly differing initial positions (end point at 0, 250 and 500 m altitude) were calculated. These ensembles (not presented here) stayed close together and indicated the low trajectory uncertainty because of the altitude of the ending point.

2.3. PM_{10} Mass Concentrations and Aethalometer Data

[7] PM_{10} mass concentrations were measured by a Tapered Element Oscillating Microbalance (TEOM, Ambient Particulate Series 1400A). Concentrations of black carbon (BC) were determined at 880 nm with a Magee Scientific Model AE30 Aethalometer, following the manufacturer's specifications [*Hansen*, 2003]. Concentration levels were derived from seven-wavelength aethalometer data measured at 5 min intervals with a sample flow rate of 5.0 LPM. Aethalometry is an optical method based on the attenuation of a beam of light transmitted through the sample collected on a fibrous filter. Thus, BC is an operational definition for the fraction of atmospheric carbonaceous material that absorbs light. Although these equivalent BC concentrations, depending notably on the knowledge of the specific mass absorption of BC, are still subject to debate [*Andreae and Gelencser*, 2006], they give a good indication of concentration levels and trends. The manufacturer's recommended absorption coefficient of BC was used, i.e., 16.6 $m^2\ g^{-1}$ for the 880 nm channel.

2.4. Aerosol Sampling on Boron Substrate and TEM Grids

[8] Atmospheric particles were collected by a cascade impactor (Dekati™ PM-10) with a flow rate of 30 L min^{-1}. The Dekati™ PM_{10} impactor has two consecutive stages to

Table 1. Criteria Used for the Identification of Particles According to Their Elemental Composition (in Atomic %) Obtained by Scanning Electron Microscopy and Elemental Energy-Dispersive X-ray[a]

Step	Criteria for Compound Identification
1	C+N+O > 75% and Ca < 5%: "Carbonaceous" - if max(Al or Si) > 5%: mix "aluminosilicate" and "carbonaceous"
2	Fe > 6%: "Fe oxide" - if C ≥ 20%: mix "carbonaceous" and "Fe oxide" - if max(Al or Si) > 5%: mix "aluminosilicate" and "Fe oxide" - if Ca > 5%: mix "Ca" and "Fe oxide"
3	Max (Cr or Mn or Ni or Zn or Pb) ≥ 5%: "Metallic" - if C ≥ 20%: mix "carbonaceous" and "metallic" - if max(Al or Si) > 5%: mix "aluminosilicate" and "metallic" - if Ca > 5%: mix "Ca" and "metallic"
4	Al+Si ≥ 10%: "Aluminosilicate" - if Si/Al ratio > 5: silica - if Mg > 5%: Mg aluminosilicate - if C ≥ 20%: mix "aluminosilicate" and "carbonaceous" - if Ca > 5%: mix "aluminosilicate" and "Ca"
5	Ca ≥ 10%: Calcite - if P > 5%: Ca-P - if Mg > 5%: Ca-Mg (dolomite) - if S/Ca ratio > 0.7 and C < 20%: gypsum - if S/Ca ratio > 0.7 and C > 19%: mix "carbonaceous" and "gypsum" - if N/Ca ratio > 0.25 and N > 5%: calcium nitrate - if max(Al or Si) > 5%: mix "aluminosilicate" and "Ca" - if Na > 5%: mix "Ca" and "marine"
6	Na > 5%: Marine - if Cl/Na ratio ≥ 0.65:sodium chloride - if S/Na ratio ≥ 0.35: sodium sulphate - if N/Na ratio ≥ 0.25 and Cl < 5% and S < 5%: sodium nitrate - if C ≥ 20%: mix "carbonaceous" and "marine" - if max(Al or Si) > 5%: mix "aluminosilicate" and "marine" - if Ca > 5%: mix "Ca" and "marine"
7	Ti > 5%: Titanium dioxide
8	The rest = Mix X/Y/Z (= ternary mixture) or Miscellaneous depending on the number of compounds internally mixed

[a]The optimized classification procedure is based on eight consecutive steps to sort all particles into eight different groups, further subdivided into single component particles and multicomponent particles (binary and ternary mixtures) to provide insight into the mixing state of particles.

separate coarse and fine fractions with equivalent cutoff diameters of 2.5 and 1 μm, each having 50% of collection efficiency. Particles impacted on a substrate material made of boron, specifically developed for the purpose of particle microanalysis [*Choël et al.*, 2005]. Transmission electron microscopy (TEM) grids with lacey carbon film were fixed on boron substrates for TEM-EELS and Raman microspectrometry analysis. Although the smallest cutoff diameter was 1 μm, particles with diameters down to 200 nm were collected and analyzed (28% of analyzed particles had an equivalent diameter smaller than 0.6 μm). Even though the collection efficiency of submicron particles is low, many particles were collected owing to their high number concentration in the air.

2.5. Automated SEM-EDX Analysis

[9] Single-particle analysis was performed with a LEO™ 438VP SEM equipped with an ultrathin-window energy-dispersive X-ray detector. Automated particle analysis was run using the commercially available Link ISIS Series 300 Microanalysis system (Oxford Instruments®). X-ray spectra were collected with an acquisition time of 20 s, at an accelerating voltage of 15 kV and a probe current adjusted to 200 pA. Atomic concentrations were calculated using a reverse Monte Carlo quantitative program [*Ro et al.*, 2003]. Average relative errors obtained with this quantification method were better than 2.5 wt %, carbon included, with effective correction of geometry effects on the whole size range (0.3–10 μm) [*Choël et al.*, 2007]. This analytical methodology was successfully tested on airborne particulate matter consisting of a complex heterogeneous mixture of particles [*Choël et al.*, 2007]. Highly volatile ammonium salts suffering from beam damage were not considered here as there was not enough information contained in their spectra. The microscope chamber was equipped with an oxygen radical source device (Evactron® RF plasma cleaner, XEI Scientific) to avoid organic carbon contamination from the pumping system and from samples. The chamber was cleaned for 15 min before the introduction of samples and 90 s in the presence of samples. This procedure proved to decrease the residual carbon content to less than 1.0 atomic percent (at. %) when tested on pure particulate inorganic compounds (analytical grade). However, high volatile organic carbon coming from samples is probably oxidized during this cleaning procedure. To obtain a good precision of the relative abundance values for minor particle groups, with relative abundance lower than 5%, a minimum number of 1000 particles per impaction stage were analyzed in each sample, as optimized in a previous study [*Choël et al.*, 2010].

[10] The identification of individual particles was based on their elemental composition obtained from SEM-EDX data, according to the criteria presented in Table 1. The procedure was performed step by step on all analyzed particles with a total of 8 steps. Threshold values of elemental concentrations for this classification procedure were determined from manual assignment of thousands of particles clearly identified as particles containing only one chemical compound. If a particle identified in a step (e.g., aluminosilicate, step 5) was already identified in a previous step (e.g., Fe oxide, step 3), it is assigned to a binary internally mixed particle type (i.e., mix aluminosilicates/Fe oxide for the previous example). It can also be identified as a ternary mixture (i.e., mix X/Y/Z) if it was previously identified as a binary mixture. Thus, the first condition given in each step (e.g., Al+Si ≥ 10% for aluminosilicate) is the necessary condition to identify the corresponding compound inside the particle of interest but, it is not sufficient to tell if this compound is the only compound present in the particle. In the last step (step 8), particles not yet identified are assigned to the miscellaneous particle type if they contain only one chemical compound (e.g., $MgCl_2$) with a minor occurrence or to the "Mix X/Y/Z" particle type if they correspond to ternary or more complex mixtures. On average, less than 1% of all analyzed particles were sorted into the miscellaneous and "Mix X/Y/Z" particle types.

2.6. Raman Microspectrometry

[11] Measurements were carried out using a confocal Raman microscope (LabRAM, Horiba Jobin Yvon) equipped with a He-Ne excitation laser (10 mW source power at 633 nm). Raman spectra of individual particles were recorded in spot analysis mode over the range 200–3500 cm^{-1} (Stokes shift), with a spectral resolution of 4 cm^{-1}, 60–120 s integration time and 5 spectral accumulations. The first-order Raman spectra of carbonaceous materials is characterized by

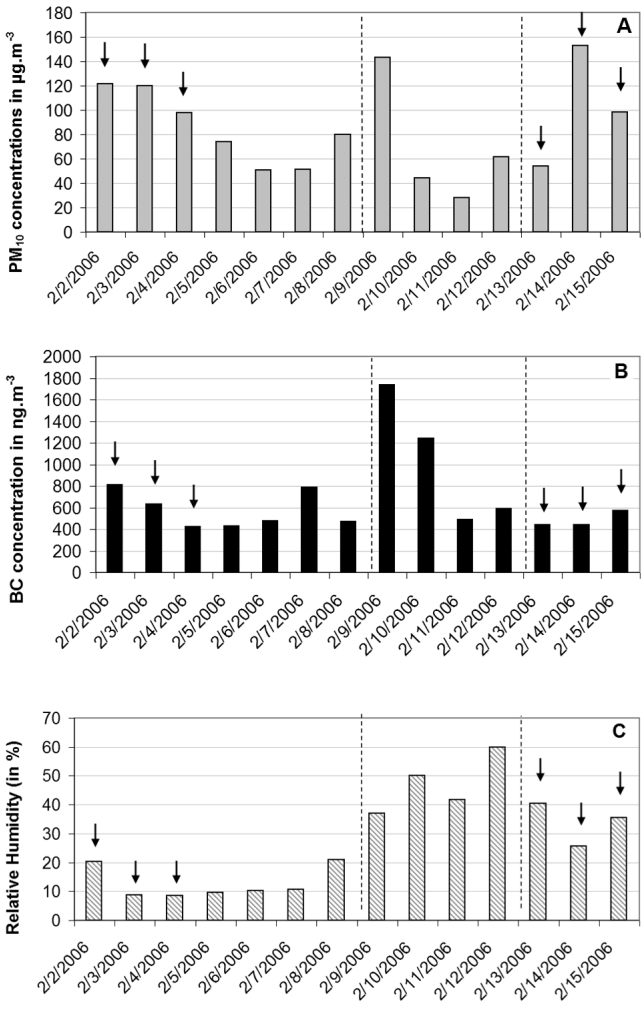

Figure 1. (a) PM_{10} concentrations, (b) black carbon (BC) concentrations, and (c) relative humidity measured during aerosol samplings. Arrows mark six specific events that were selected for a detailed characterization of the mixing state of aerosols.

two broad and overlapping bands with intensity maxima around 1580 cm^{-1}, denoted "G" (graphite peak), attributed to ideal graphitic lattice (E_{2g} symmetry) stretching mode, and 1350 cm^{-1}, denoted "D" (disorder peak), associated to disordered graphitic lattices [*Tuinstra and Koenig*, 1970]. For structural characterization of soot and related carbonaceous materials, Raman spectra were fitted as proposed by *Sadezky et al.* [2005] with a combination of five Lorentzian-shaped bands, denoted G, D1, D2, D3 and D4, at about 1580, 1350, 1620, 1500, and 1180 cm^{-1}, respectively, and compared to reference spectra.

2.7. TEM-EELS Observations

[12] The structure, morphology and chemical composition of the most abundant types of particles were manually analyzed by transmission electron microscopy (TEM) and electron energy loss spectroscopy (EELS). High-resolution electron images and EELS spectra were obtained using a JEOL-2010F TEM equipped with a Gatan GIF system. EELS spectra were acquired using a 0.5 eV/ch dispersion leading to an energy range of about 510 eV per spectrum. Carbon structural variations in atmospheric carbonaceous particles can be determined from the C K-edge of energy loss spectra by the relative amounts of σ^* and π^* bondings [*Braun et al.*, 2005; *Hopkins et al.*, 2007; *Katrinak et al.*, 1992]. The 1 s transition to the π^* conduction band occurs at 285.5eV, whereas the 1 s transition to the σ^* conduction band occurs at a significantly higher energy loss, at about 290 eV or higher depending on bond distance. Therefore, spectra with higher π^*/σ^* ratios indicate more π bonding and thus structure with a greater graphitic character. Moreover, the σ^* peak is tall and sharp with a characteristic fine structure of the shape just after the peak when structural ordering occurs as in the graphite spectrum, whereas amorphous carbon gives a broad peak with a smooth shape.

3. Results and Discussion

[13] PM_{10} and black carbon (BC) mass concentrations and relative humidity (RH) are considered (Figure 1) to evaluate the relative influence of marine, dust and human emissions on the atmospheric abundance and chemical composition of aerosols at the sampling site. Although no large dust events were sampled, PM_{10} mass concentrations (Figure 1a) are essentially influenced by supermicrometer particles composed of mineral dust like in major African source areas of Aeolian soil dust (northeast desert in Niger or the Bodélé depression in Chad) [*Rajot et al.*, 2008]. At our coastal site, marine particles may also be dominated by the coarse fraction of aerosols. The occurrence of marine air masses can be indicated by an increase of the relative humidity (Figure 1c), as observed for the samples collected during the period from 9 to 12 February 2006 associated with marine air masses (Figure 2). Finally, BC concentrations (Figure 1b) can give an indication on the abundance of carbonaceous particles or more precisely soot, the dominant light absorbing aerosol species. Vehicle fuels in western Africa are very polluting because of their poor quality and generate severe atmospheric pollution [*van Vliet and Kinney*, 2007]. BC hourly concentration profiles recorded at M'Bour are in accordance with traffic, with 3 maxima at about 0800, 1600 and 2000 UT that can get up to 4000 $ng.m^{-3}$. Our measurements were performed each day between 1200 and 1300 UT, out of the high traffic periods, when BC concentrations are relatively low (Figure 1). Taken into account all these parameters (RH, PM_{10} and BC concentrations) and meteorological data, 6 events were selected from the dry season Special Observation Period (AMMA SOP-0), as representative of the atmospheric matter leaving the coastal Sahelian zone and transported over Atlantic Ocean during dry season, except during large dust events. The period from 9 to 12 February 2006 was avoided because it could be strongly influenced by local emissions from the densely populated West African coast and more particularly the city of M'Bour (Figure 2). The 6 selected events correspond to the highest PM_{10} concentrations for the two other periods, and variable RH and BC concentrations (Figure 1, marked events). The nighttime BC background ranged from about 150 ng m^{-3} for samples collected during the period 13–15 February, to about 700 ng m^{-3} for samples collected from 2 to 4 February. These background values are much higher than BC concentrations measured at remote sites

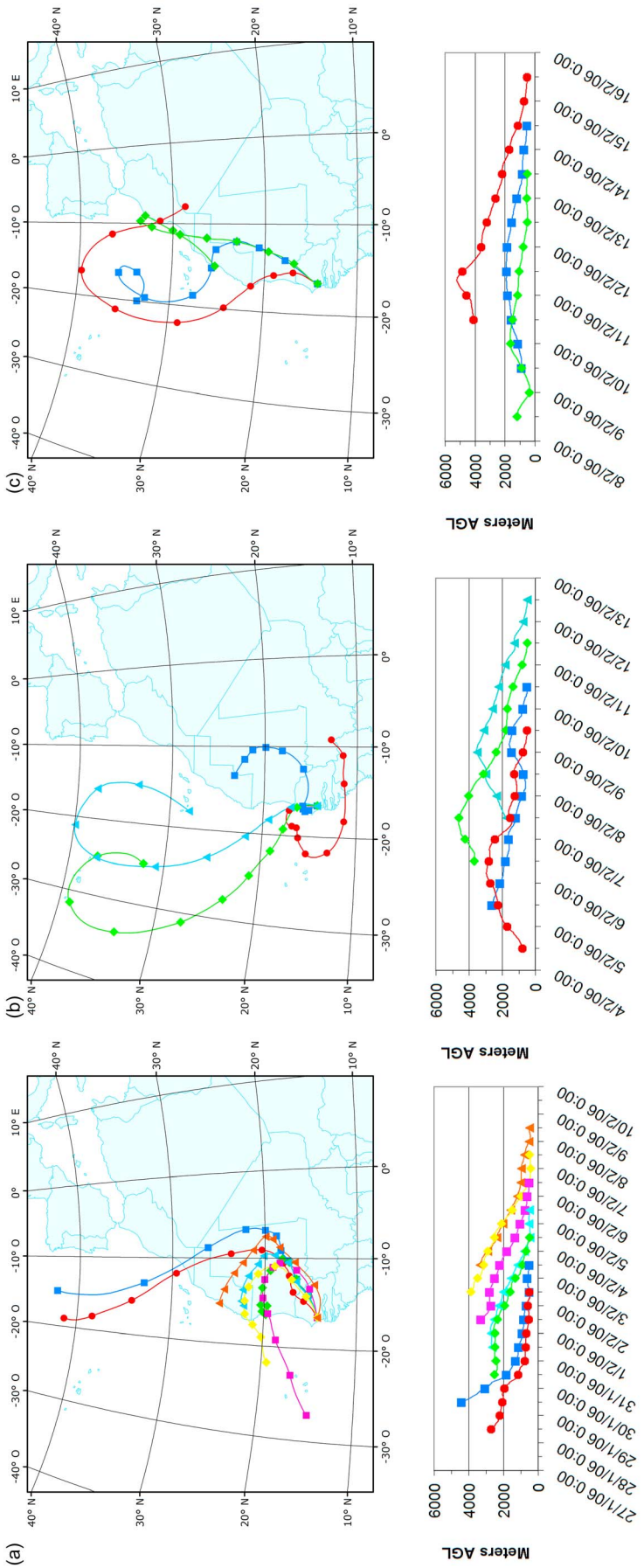

Figure 2. The 120 h backward trajectories of air masses sampled (a) from 2 February to 8 February 2006, (b) from 9 February to 12 February 2006, and (c) from 13 February to 15 February 2006.

Table 2. Relative Abundances of Externally Mixed, Binary Internally Mixed, and Ternary Internally Mixed Particles for Six Selected Events[a]

Particles	2 Feb	3 Feb	4 Feb	13 Feb	14 Feb	15 Feb
Externally mixed particles	82.1%	89.5%	75.7%	51.5%	83.5%	73.8%
(dust, carbonaceous and marine particles)	(1477)	(2017)	(1726)	(1002)	(1838)	(1617)
Binary internally mixed particles	17.2%	10.5%	24.3%	46.5%	16.1%	25.1%
(mixed carbonaceous/dust, mixed carbonaceous/marin, and mixed dust/marine particles)	(310)	(236)	(554)	(905)	(355)	(550)
Ternary internally mixed particles	0.7%	0.0%	0.0%	2.0%	0.4%	1.1%
(mixed carbonaceous/dust/marine particles)	(12)	(1)	(0)	(38)	(9)	(25)
Total	100%	100%	100%	100%	100%	100%
	(1799)	(2254)	(2280)	(1945)	(2202)	(2192)

[a]See Figure 1. The number of analyzed particles is reported in parentheses.

[*Bhugwant and Brémaud*, 2001] and regional and/or continental anthropogenic emissions should be considered in the following discussion concerning these 6 events.

3.1. Mixing State of Aerosol

[14] An overview of mixing states of atmospheric particles obtained from SEM-EDX data is presented in Table 2. Externally mixed particles are defined here as particles containing only one chemical compound according to the identification criteria reported in Table 1. Aluminosilicate, silica, calcite, iron oxide, gypsum, titanium dioxide, carbonaceous, sodium chloride and sodium nitrate particles are identified as externally mixed particles (Table 3). However, they also often contain unexpected elements in a low fraction (less than 3 at. %, excluding carbon), like aluminum and silicon in the case of calcium carbonate particles. Moreover, they contain on average a significant fraction of carbon ranging from 6.3 to 11.3 at. %. Since volatile and semivolatile carbonaceous compounds are eliminated by the oxygen plasma cleaner of the microscope, the residual carbon content does not come from volatile organic carbon, but rather from higher molecular mass compounds, more resistant to oxidation reactions during the oxygen plasma cleaning, like graphite carbon, humic substances, heavy aliphatic or aromatic compounds. In fact, truly pure particles are quasi-nonexistent in the atmosphere. If stricter criteria were set for the particle identification, almost all atmospheric particles would be considered as unique mixtures of different compounds, practically impossible to interpret. Because of their volatilities, ammonium sulfate particles were not included in this discussion.

[15] Dust, carbonaceous and marine compounds are mostly found externally mixed (Table 2), i.e., not present in the same particles. The particles containing internally mixed crustal compounds (e.g., iron enriched or calcium enriched aluminosilicates) are also assigned to the dust particle category. Dust, marine and carbonaceous particles account for respectively 78, 12 and 9% of externally mixed particles. The chemical composition of dust depends on the soil type in the source region. Considering the trajectories of sampled air masses (Figure 2), most of dust particles associated to the selected events probably come from northwestern Sahara. According to the literature, mineral dust transported from deserts of North Africa are rich in calcite and dolomite, whereas mineral dust emitted from Niger and Mauritania are rich in iron oxides [*Formenti et al.*, 2003]. The presence of a significant fraction of calcite particles (Table 3; about 11% of dust particles) and a very low fraction of iron oxide particles (about 1% of dust particles) in our mineral dust samples with an origin in the northwestern Sahara corroborates this. C particles are relatively small particles compared to mineral dust: the mean equivalent diameter of C and dust particles analyzed by SEM-EDX are respectively 0.66 μm (1 SD = 0.66 μm) and 1.17 μm (1 SD = 1.11 μm). This is consistent with the formation of carbonaceous particles by gaseous phase condensation in the near field of incomplete combustion (primary particles) or during atmospheric transport (secondary organic particles), while mineral dust particles are generated in the atmosphere by mechanical wind erosion of soils [*Seinfeld and Pandis*, 1998]. Among marine particles, sodium chloride and sodium nitrate compounds account for about 12% of externally mixed particles, with mean equivalent diameters of 1.75 μm (1 SD = 1.51 μm) and 1.27 μm (1 SD = 0.81 μm), respectively. Supermicrometer particles are thus predominant in the marine particle group.

Table 3. Elemental Composition of Externally Mixed Particles

Compound	Total Number of Particles	Particle Type[a]	Average Chemical Composition (in Atomic %)[b]
Aluminosilicate	4954	D	C(8.4) **O(57.3)** Mg(1.4) **Al(11.3) Si(15.8)** Fe(1.8)
Calcium carbonate	755	D	**C(20.3) O(55.4)** Na(1.1) Mg(1.1) Al(1.5) Si(2.1) **Ca(16.0)**
Carbonaceous	776	C	**C(82.8) O(11.3)** Si(1.0)
Gypsum	106	D	C(7.6) **O(60.2)** Na(1.7) Mg(1.2) Al(1.0) Si(1.4) **S(12.8) Ca(12.1)**
Iron oxide	75	D	C(7.6) **O(61.0)** Al(2.6) Si(2.6) **Fe(22.0)**
Mg Aluminosilicate	187	D	C(8.2) **O(55.2) Mg(8.5) Al(6.5) Si(15.8)** Fe(1.8)
Silica	636	D	C(6.3) **O(58.0)** Al(2.4) Si**(30.4)**
Sodium chloride	645	M	C(8.9) O(16.8) **Na(38.4)** Mg(1.9) **Cl(29.5)**
Sodium nitrate	366	M	C(6.7) **N(12.1) O(51.8) Na(21.3)** Mg(1.9) Al(1.2) Si(1.5)
Titanium oxide	58	D	C(11.3) **O(57.4)** Al(2.6) Si(3.0) **Ti(21.4)** Fe(1.3)

[a]D, dust particles; C, carbonaceous particles; M, marine particles.
[b]Major elements are in bold. Only elements with mean concentrations higher than 0.9 atomic % are reported.

[16] Binary internally mixed particles can also account for a high proportion (from 10.5 to 46.5% of analyzed particles), whereas the relative abundances of ternary internally mixed particles are always very low, with a maximum of 2% of analyzed particles for the sample collected on 13 February 2006. Relative abundances of individual particles sorted into external (i.e., carbonaceous, dust, or marine) and binary internal mixture types (i.e., mixed carbonaceous/dust, mixed dust/marine, mixed carbonaceous/marine) are presented in Figure 3. Considering all events, the major internal binary mixtures are mixed carbonaceous/dust and dust/marine particles. Although carbonaceous particles have always the lowest mean diameters, the comparison of the mean diameters of mixed carbonaceous/dust particles with those of dust particles do not reveal a clear tendency. Sometimes they are lower than those of dust particles (as for 3, 4, and 15 February 2006), and in the others cases they are higher. On the same way, no systematic significant relation (Mann-Whitney test, $p = 0.05$) between the mean diameters of mixed dust/marine particles and those of dust or marine is observed.

3.2. Scavenging of Marine Compounds by Dust

[17] Regarding the six selected events, particles containing marine compounds are relatively abundant when relative humidity is equal to, or higher than 20% (samples collected on 2 and 12–15 February 2006). For these four cases, the ratio of mixed marine (with dust or carbonaceous compounds) to "pure" marine particles ranges from 0.7 to 3.3. Marine compounds are thus often associated with other compounds to form mixed particles. The elemental mappings of mixed dust/marine particles, illustrated in Figure 4, indicate that aluminosilicate particles are often completely coated by marine compounds (principally $NaNO_3$ in Figure 4). This coating was confirmed by Raman microspectrometry observations. These mixed particles, already observed in other studies [*Ma et al.*, 2004; *Sullivan et al.*, 2007], were probably formed by coagulation of dust and marine particles. The ambient relative humidity during sampling (Figure 1) is lower than the efflorescence relative humidity (ERH) of micrometer-sized NaCl particles (45 ± 3%), but sea-salt particles are probably liquid since ERH drastically decreases in the presence of organic compounds [*Gao et al.*, 2008], as suspected for our marine particles that systematically contain some carbon (Table 3). Deliquescence can affect physical processes. Coagulation processes can easily take place between particles in a deliquescent state. Moreover, the homogeneous distribution of marine compounds at the surface of dust could be explained by cloud processes: at high relative humidity, mixed dust/marine particles could evolve into a solid core (the insoluble mineral dust particle) completely coated by a liquid salt layer. Consequently, when the relative humidity decreases under the crystallization point, solid sea salts are homogeneously distributed at the surface of particles. The back trajectories of sampled air masses were calculated using the HYSPLIT model with dumping RH data along them (not presented here). These calculations highlight that for the last studied period (13–15 February 2006), when dust particles are mostly mixed with sea salts (Figure 3), more than 60% of time trajectories are associated with RH higher than 70%. That corroborates the hypothesis of a homogenisation of the sea-salt distribution at the surface of dust particles by deliquescence of salts. The rate of aggregation of marine compounds on dust particles does not seem to be linked with the residence time of sea-salt particles in the atmosphere. Newly formed sea salts are mainly composed of genuine NaCl. They can react in polluted air masses with gaseous species such as H_2SO_4 or/and HNO_3 to form partly or completely converted sea salts [*Finlayson-Pitts and Pitts*, 2000]. Completely converted sea salts are characterized by the absence of chloride, lost to the gas phase as HCl, and are typically composed of Na_2SO_4 or/and $NaNO_3$. 98.7% of marine particles are partially or totally converted sea salts for the sample collected on 14 February 2006. These particles are not local sea-salt particles freshly emitted since they had time to be converted during their atmospheric transport. Such aged marine particles only represent 41.5, 54.4 and 63.8% of marine particles for samples collected on 13, 15 and 2 February, respectively. And yet, the relative abundances of mixed compared to pure marine particles are not significantly lower for these last 3 samples, evidencing the rapid aggregation of sea salts with dust. Other parameters like relative humidity and atmospheric turbulence have probably a key role on the mixing state of marine particles with dust. This scavenging of marine compounds by dust has a large impact on their optical properties. During the long-range transport of Saharan air masses over the Atlantic Ocean, the formation probability of mixed dust/marine particles is significant, as observed by *Worobiec et al.* [2007] for soil dust particles collected in the Amazon Basin and coming from the Sahara. These hygroscopic mixed particles have a spectral absorption of solar radiation different than that of pure dust particles. The high capacity of marine particles to mix with dust has to be considered in the radiative budget calculation.

3.3. Scavenging of Carbonaceous Compounds by Dust

[18] In western Africa, gaseous and particulate carbonaceous compounds (excluded carbon monoxide and dioxide) are predominantly of anthropogenic origin. Two major key sources can be distinguished: The widespread burning of agricultural biomass, notably during December–February, first constitutes a large source of carbonaceous pollutant in the North African continent [*Johnson et al.*, 2008]. Second, urban emissions from growing African cities can largely contribute to atmospheric carbonaceous compounds inventory, because of vehicle fleets, high per vehicle emissions, limited road infrastructure and road congestion [*van Vliet and Kinney*, 2007]. This urban source also includes domestic charcoal and wood fires used for cooking. All these combustion sources generate both gaseous and particulate carbonaceous compounds that can interact by condensation or aggregation with mineral dust particles during atmospheric transport to form mixed carbonaceous/dust particles. For all the measured events, mixed carbonaceous/dust particles collected at M'Bour are relatively more abundant than pure carbonaceous particles (Figure 3). Even if the condensing material is not the same as the unmixed primary carbon material, the identification of these pure carbonaceous particles can give insights into the origin of carbonaceous compounds constituting internally mixed carbonaceous particles. More than 60% of analyzed pure carbonaceous particles (C particles) contain more than 90 at.% of carbon and are associated with a low oxygen content (1.7 at.% on average). This suggests freshly emitted C particles, not oxygenated by photochemical processes. For the others C particles (containing relatively high oxygen

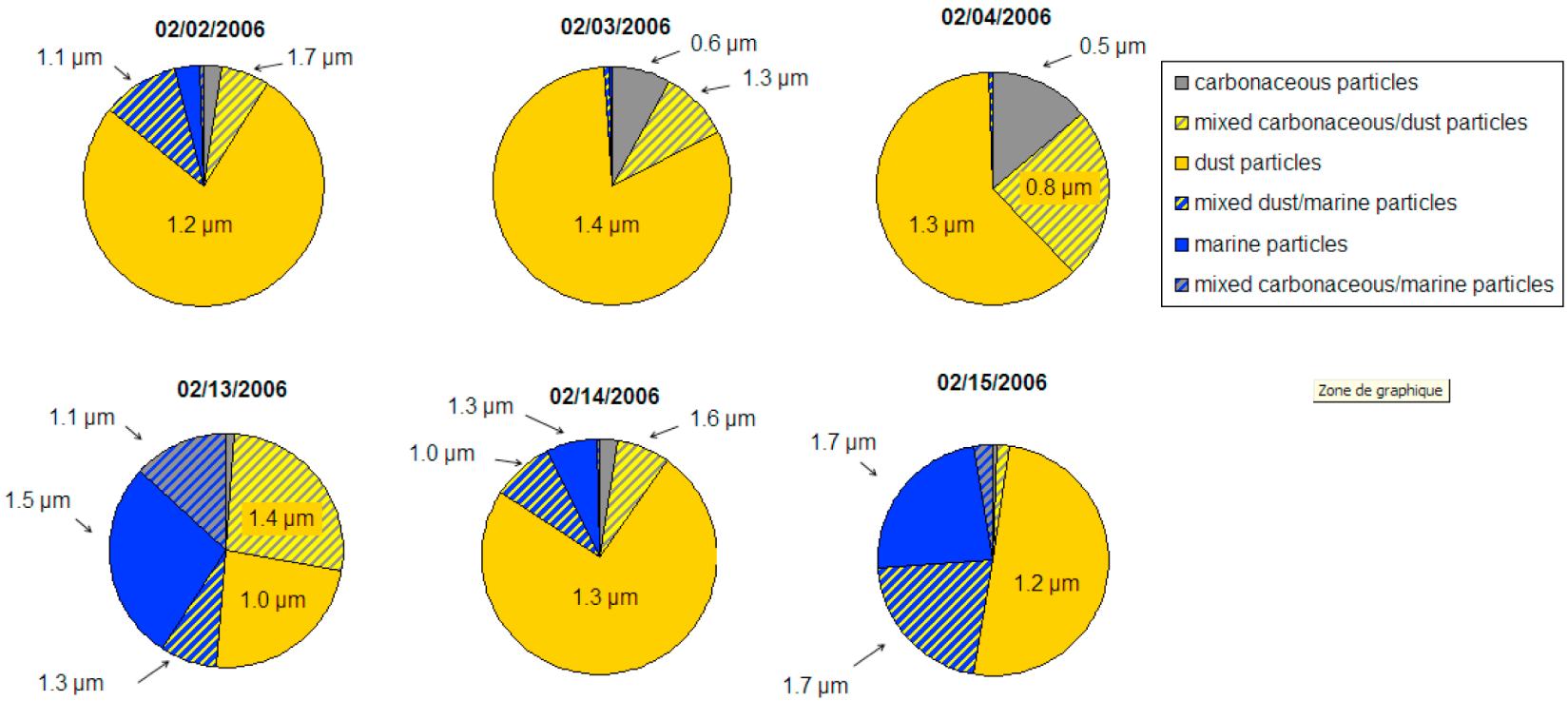

Figure 3. Relative abundances of individual particles sorted into external (i.e., carbonaceous, dust, or marine) and binary internal mixture types (i.e., mixed carbonaceous/dust, mixed dust/marine, mixed carbonaceous/marine) for six selected events (see Figure 1). Ternary internally mixed carbonaceous/dust/marine particles are not considered here. The average diameter of particles is indicated for categories accounting for more than 100 particles.

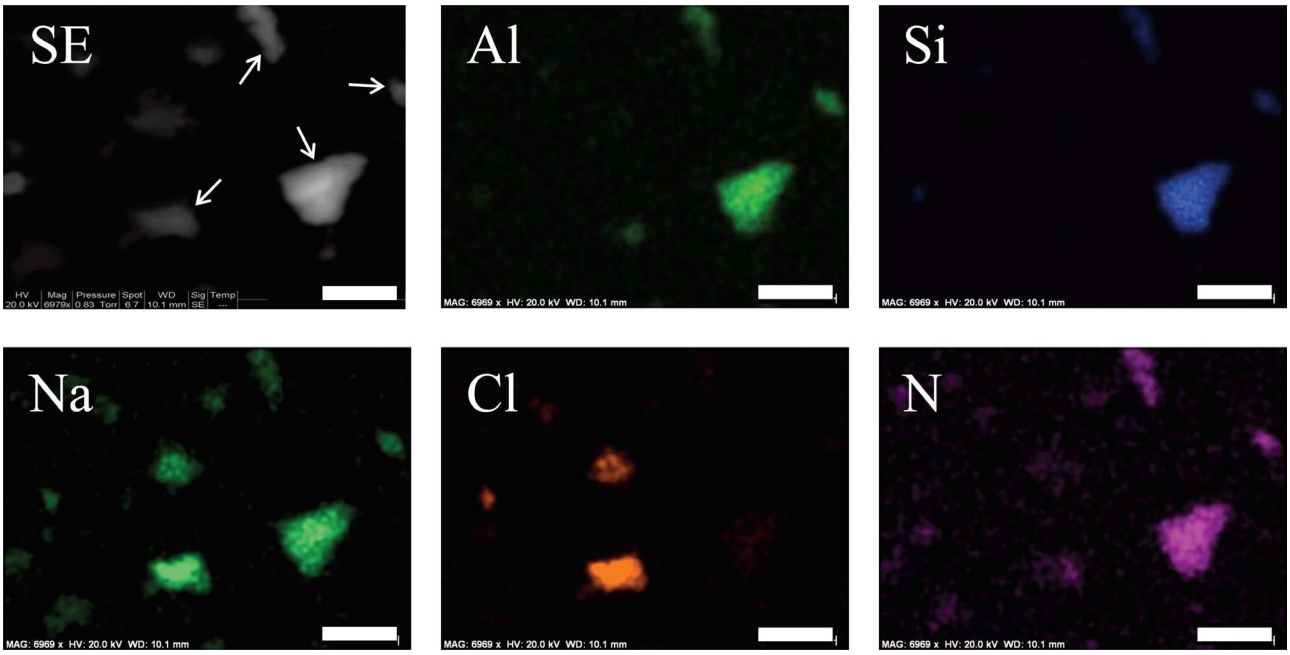

Figure 4. Scanning electron microscopy (SEM) image and elemental energy-dispersive X-ray (EDX) mappings (Al, Si, Na, Cl, and N) of individual internally mixed dust/marine particles (marked with white arrows). Scale marker bars correspond to 4 μm.

content), stochiometric calculations indicate that this oxygen is due to the presence of inorganic impurities like aluminum, silicon or sulphur that are in an oxidized form. Morphological parameters obtained by electron microscopy allow two major kinds of C particles to be distinguished: Soot with a fractal-like chain structure, and tar balls identified as separate spherules (Figure 5). The low intensity of the oxygen edge in EELS spectra of soot and tar balls (Figure 5) confirms the low oxygen content of carbonaceous compounds.

[19] Soot accounts for an important fraction of the C particles. They are known to be a chemically complex mixture of amorphous carbonaceous compounds and graphitic elemental carbon [*Buseck et al.*, 1987]. The crystallinity and the graphitic nature of soot depend upon the conditions of the combustion process in which they were formed [*Roessler et al.*, 1981]. High-resolution TEM images of soot particles collected at M'Bour (Figure 5b) show no structural organization and no observation of nanocrystalline graphite with an onion shell structure as sometimes mentioned in the literature [*Pósfai et al.*, 2003; *Wentzel et al.*, 2003]. However, the 1 s $\rightarrow \sigma^*$ peak of the carbon edge on EELS spectra (Figure 5b) is systematically sharp and tall, indicating a high proportion of sp^2 hybridized carbon, but the following fine structure of the shape is smoothed compared to the C-K edge of graphite spectra [*Bernier et al.*, 2008; *Gloter et al.*, 2003], so the structural ordering is not extended.

[20] The other major type of C particles is tar balls. They are exclusively observed in biomass burning and biofuel emissions and absorb light in the UV, visible and near-IR regions of the electromagnetic spectrum [*Alexander et al.*, 2008; *Hand et al.*, 2005; *Pósfai et al.*, 2004]. They are spherical and amorphous C particles (Figure 5a) and typically not aggregated with other particles. The carbon edge of tar balls in EELS spectra is typical of amorphous carbon. Potassium containing particles, generally associated with C particles when they come from biomass burning and natural forest fires [*Chou et al.*, 2008; *Liu et al.*, 2000; *Pósfai et al.*, 2003], were not significantly encountered in our samples. The biomass burning origin of these C particles is unquestionable but they could come from domestic wood fire rather than forest fire because of the absence of potassium containing particles [*Echalar et al.*, 1995]. The low K concentrations obtained from bulk analysis (not presented here) in associated PM_{10} samples and the absence of long-range transport of air masses from equatorial Africa (Figure 2) where intensive forest fires generate biomass burning aerosols confirm this. In conclusion, C particles collected at M'Bour during the dry season (both soot and tar balls) are likely to have come from urban emissions, probably from Dakar and other neighboring densely populated areas. Carbonaceous compounds associated with mixed carbonaceous/dust particles probably come from the same urban areas.

[21] The formation of carbonaceous particles by combustion processes is accompanied by the emission of numerous volatile and semivolatile organic compounds and mixed dust/carbonaceous particles could be formed in the atmosphere by two different physical processes: on the one hand, carbonaceous compounds could condense on dust particles to form a carbonaceous layer. Indeed, volatile and semivolatile organic compounds can adsorb onto dust particles when a dust plume is mixed with polluted plumes containing emissions from human activities, forests or marine areas [*Usher et al.*, 2003] and form a carbonaceous coating. On the other hand, carbonaceous particles (more probably tar balls or soot particles in our study) could coagulate with dust particles to form carbonaceous aggregates at the surface of dust particles. Organics were often found mixed with sulphates in atmospheric particles [*Buseck and Pósfai*, 1999; *Ebert et al.*, 2004;

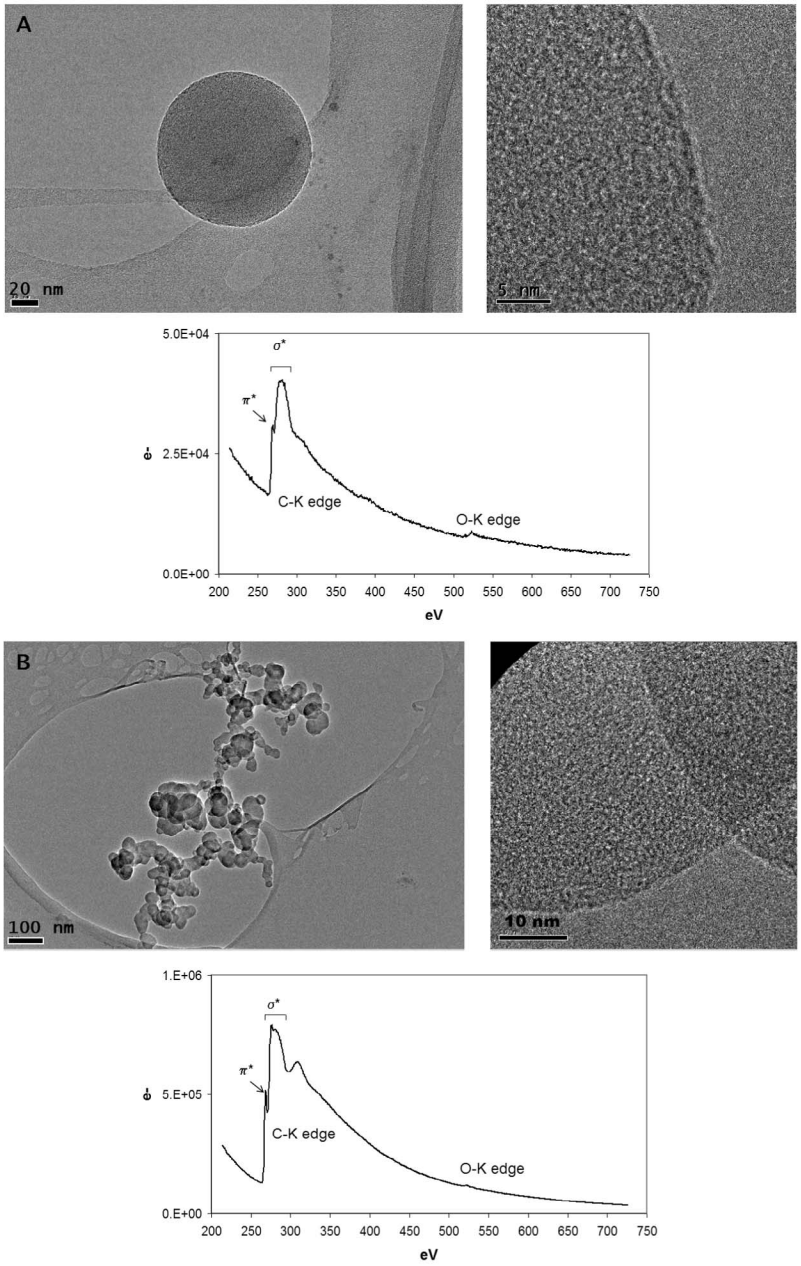

Figure 5. Transmission electron microscopy (TEM) image of (a) a spherical tar ball and (b) soot particles on a lacey carbon film with corresponding high-resolution TEM images and electron energy loss spectroscopy (EELS) spectra.

Lee et al., 2002] and only few studies reported the presence of organic compounds on mineral dust particles [*Falkovich et al.*, 2004; *Hobert*, 1995; *Russell et al.*, 2002]. *Leaitch et al.* [2009] notably observed carbonaceous compounds attached to coarse dust particles, suggesting a scavenging of organic compounds by Asian dust near anthropogenic sources. *Arimoto et al.* [2006] observed that Asian dust collected below about 2 km altitude during ACE-Asia was commonly mixed with carbonaceous pollutants, to give a mixing with black carbon by aggregation. The presence of light-absorbing carbonaceous matter on mineral dust particles is important since it can strongly affect the light absorption spectrum, hence the radiative impact of dust [*Kirchstetter et al.*, 2004]. The sp^2-hybridation in graphitic carbon contained in soot or black carbon is related to photoabsorption and index of refraction [*Bond and Bergstrom*, 2006]. The aggregation of soot particles with mineral dust will increase the light absorption of these dust particles and the magnitude of their contribution to radiative forcing. But other carbonaceous compounds, also called "brown carbon," can also significantly contribute to light absorption with strong wavelength dependence, even if they constitute weak-absorbing compounds [*Andreae and Gelencser*, 2006]. As illustrated for a typical mixed carbonaceous/dust particle collected at M'Bour (Figure 6), the elemental EDX mappings seem to indicate that carbon is homogeneously distributed over the surface of

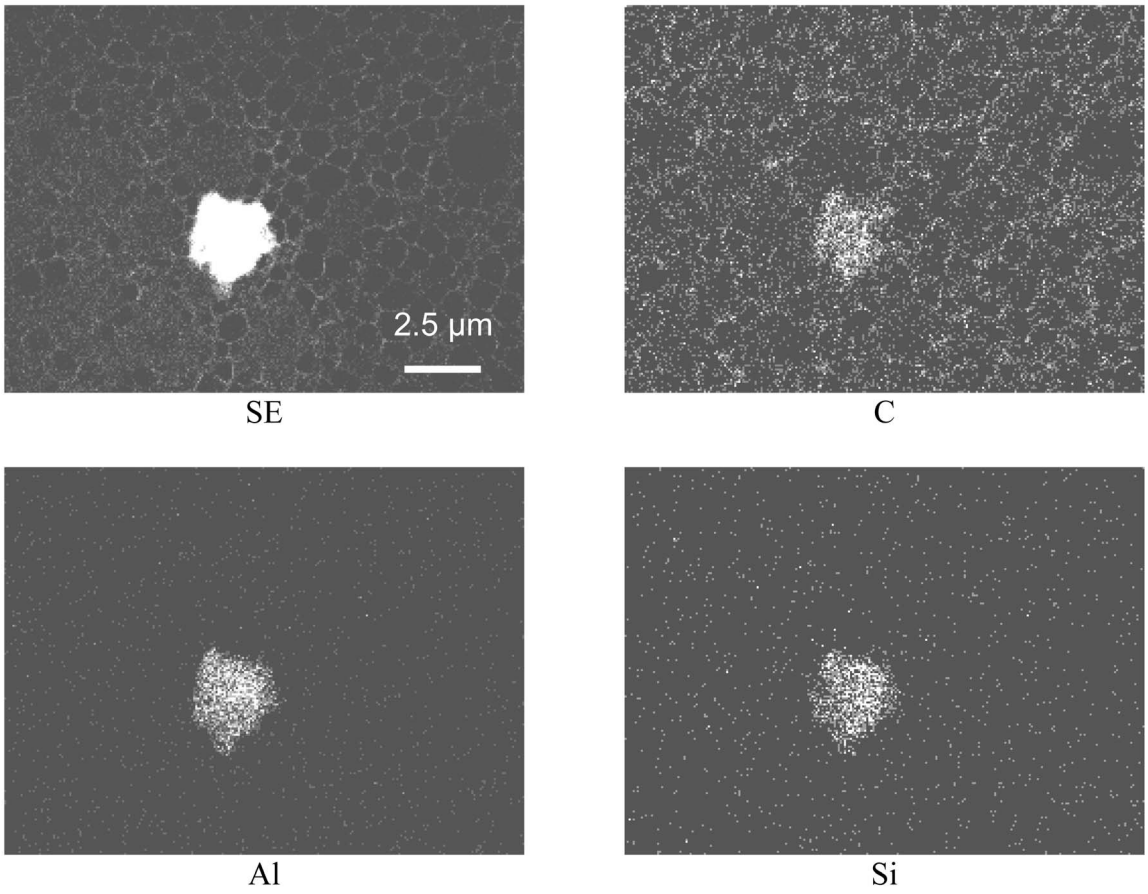

Figure 6. SEM image and elemental EDX mappings (Al, Si, and C) of a mixed carbonaceous/dust particle on lacey carbon film.

particles. Although the lacey carbon film reduces the sharpness of the C maps, the perimeter of the mixed carbonaceous/dust particles is always very similar to that on the Al or Si maps. A typical Raman spectrum of a mineral dust particle identified as internally mixed with carbonaceous compounds from previous SEM-EDX analysis is presented in Figure 7. Curve fitting of the first-order spectral region characteristic of carbonaceous species (800–2000 cm^{-1}) was carried out using five band fits (denoted G, D1, D2, D3, and D4). The D1 band full width at half maximum (FWHM) enables a clear distinction of carbonaceous materials with variable degree of structural order [*Ivleva et al.*, 2007]. Figure 8 reports experimental values of D1 band FWHM for five reference samples (i.e., highly oriented pyrolytic graphite, graphite flakes, activated carbon, urban soot and SRM 1650b diesel soot) and nine individual mineral dust particles in the size range 1.5–2.8 μm, identified as internally mixed with carbonaceous compounds from previous SEM-EDX analysis. The average value of the D1 band FWHM for African dust particles was found at 195 cm^{-1}, close to the values obtained for urban soot and diesel soot reference samples, found at 173 and 175 cm^{-1}, respectively. Such high D1 band FWHM indicates a low degree of graphitization (prevalence of amorphous domains). The absence of fractal shape for these mixed carbonaceous/dust particles evidenced by TEM observations and a smooth shape of the broad carbon edge in their EELS spectra, typical from amorphous carbon, exclude an aggregation of dust with soot particles. Therefore, the high D1 band FWHM in Raman spectra is consistent with the formation of an amorphous coating by adsorption of carbonaceous compounds on mineral dust particles during their atmospheric transport. These carbonaceous compounds could be constituted from carboxylic

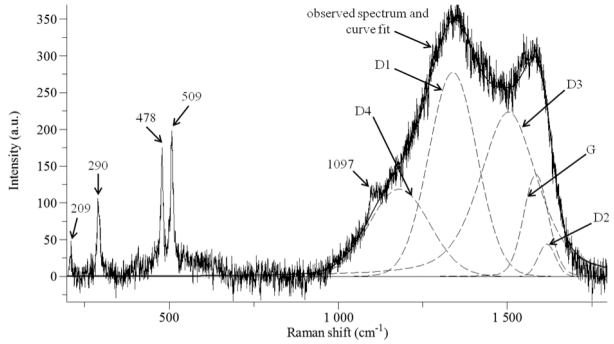

Figure 7. Typical Raman spectrum of a mineral dust particle internally mixed with carbonaceous compounds. The mineral particle is composed of dolomite, identified at 209 and 1097 cm^{-1}, and Na-feldspar, identified at 290, 478, and 509 cm^{-1}. Curve fitting of the first-order spectral region characteristic of carbonaceous species (800–1800 cm^{-1}) was carried out with five band fits (G, D1, D2, D3, D4).

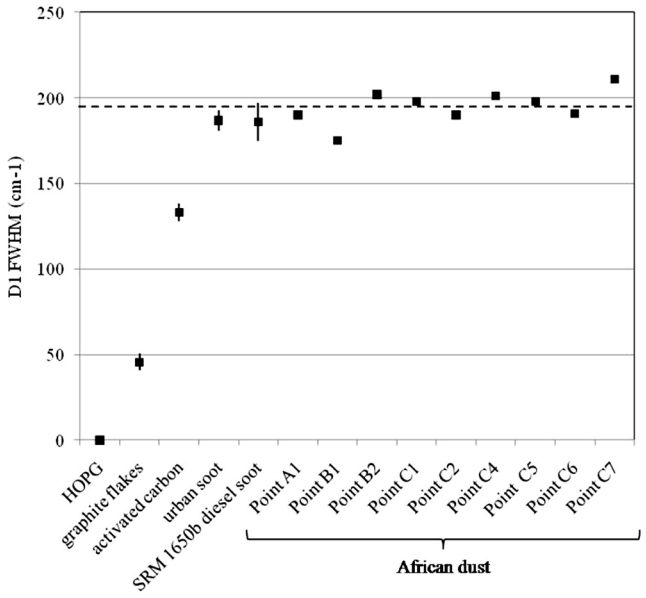

Figure 8. Full widths at half maximum (FWHM) of the D1 band for five reference samples and nine individual African dust particles (mean values ± standard deviations) identified as internally mixed with carbonaceous compounds from previous SEM-EDX analysis. HOPG stands for highly oriented pyrolytic graphite. The dashed line corresponds to the average value of D1 band FWHM for the African dust particles.

acids as already observed in other studies [*Sullivan and Prather*, 2007; *Takahama et al.*, 2010].

[22] In conclusion, mixed dust/carbonaceous particles observed at M'Bour are probably the result of adsorption on dust particles of organic compounds from local anthropogenic emissions. These emissions can come from domestic wood fire or urban activities as suspected for pure carbonaceous particles. Moreover, volatile carbon and/or inorganic materials like sulphate were also probably present at the surface of atmospheric particles but were lost in the analytical process. As a light-absorbing component of aerosols, the carbonaceous coating probably plays an important role in the radiative properties of the atmosphere. Moreover, such carbonaceous coating (as volatile compounds probably associated with it) can affect the cloud condensation nuclei (CCN) behavior of the core dust, considering the higher hygroscopicity of carbonaceous compounds in the outer layer relative to that of mineral dust [*Takahama et al.*, 2010].

4. Summary and Conclusion

[23] The purpose of this study was to describe the mixing state of African dust collected in Senegal during the dry season, combining complementary microanalytical tools. The identification of individual particles was based on their elemental composition obtained from SEM-EDX data. To avoid considering all particles as unique mixtures of different compounds, the definition of externally mixed particles used in this work includes some limited internal mixing: externally mixed particles often contain unexpected elements in a low fraction (ranging from 6.3 to 11.3 at.% for carbon and less than 3 at.% for the other elements). The chemical composition and relative abundances of externally mixed particles gave insights into the origin of compounds constituting internally mixed particles. Externally mixed particles are essentially composed of mineral dust, carbonaceous and marine particles. All together, mineral dust, carbonaceous and marine particles represent 76% of the total number of analyzed particles. The other particles are internally binary or ternary mixed particles (23% and 1% of the total number of analyzed particles, respectively). Depending on a given sample, binary internally mixed particles can account for a high proportion: up to 46.5% of analyzed particles. They are more often mixed carbonaceous/dust and mixed dust/marine particles. The mixed dust/marine particles were probably formed by coagulation. Aluminosilicate particles are completely coated by marine compounds (principally $NaNO_3$), probably because of cloud processes. Carbon is homogeneously distributed at the surface of mixed carbonaceous/dust particles, providing evidence of coated carbonaceous compounds within dry atmospheric particles. Raman microspectrometry observations at the particle scale highlight an amorphous rather than crystallized carbon structure of the carbonaceous coating on African dust. Volatile and semivolatile organic compounds from urban emission probably adsorbed on dust particles to form mixed dust/carbonaceous particles. This coating certainly modifies hygroscopic properties [*Pósfai et al.*, 1998], hence optical properties of mineral dust [*Takahama et al.*, 2010].

[24] **Acknowledgments.** On the basis of a French initiative, the AMMA project was built by an international scientific group and is currently funded by a large number of agencies, especially from France, the United Kingdom, the United States, and Africa. It has been the beneficiary of a major financial contribution from the European Community's Sixth Framework Research Programme. Detailed information on scientific coordination and funding is available on the AMMA International web site http://www.amma-international.org. The authors are very thankful to the LISA staff and notably Bernadette Chatenet for managing the M'Bour long-term site, for providing local meteorological data, and for the acquisition of the TEOM. Also we thank Tamsir Diop, Aboubacri Dialo, and the staff of the Institut de Recherche et Développement (IRD) for their helpful contribution to our instrument installation. We are very grateful to V. Cornille, X. Mériaux, D. Tanré, T. Potdvin, F. Auriol, A. Bory, and D. Malengros for their technical help during the campaign and its preparation. The authors thank the NOAA Air Resources Laboratory (ARL) for the provision of the HYSPLIT transport and dispersion model and the READY web site used in this publication (http://www.arl.noaa.gov/ready.html). Finally, we would like to thank the three anonymous reviewers for their helpful comments on the manuscript.

References

Alexander, D. T. L., P. A. Crozier, and J. R. Anderson (2008), Brown carbon spheres in east Asian outflow and their optical properties, *Science*, *321*(5890), 833–836, doi:10.1126/science.1155296.

Andreae, M. O., and A. Gelencser (2006), Black carbon or brown carbon? The nature of light-absorbing carbonaceous aerosols, *Atmos. Chem. Phys.*, *6*, 3131–3148, doi:10.5194/acp-6-3131-2006.

Arimoto, R., et al. (2006), Characterization of Asian dust during ACE-Asia, *Global Planet. Change*, *52*(1–4), 23–56, doi:10.1016/j.gloplacha.2006.02.013.

Batonneau, Y., S. Sobanska, J. Laureyns, and C. Brémard (2006), Confocal microprobe Raman imaging of urban tropospheric aerosol particles, *Environ. Sci. Technol.*, *40*, 1300–1306, doi:10.1021/es051294x.

Bernier, N., F. Bocquet, A. Allouche, W. Saikalyd, C. Brosset, J. Thibault, and A. Charai (2008), A methodology to optimize the quantification of sp2 carbon fraction from K edge EELS spectra, *J. Electron Spectrosc. Relat. Phenom.*, *164*, 34–43, doi:10.1016/j.elspec.2008.04.006.

Bhugwant, C., and P. Brémaud (2001), Simultaneous measurements of black carbon, PM10, ozone and NOx variability at a locally polluted island in the southern tropics, *J. Atmos. Chem.*, *39*, 261–280, doi:10.1023/A:1010692201459.

Bond, T. C., and R. W. Bergstrom (2006), Light absorption by carbonaceous particles: An investigate review, *Aerosol Sci. Technol.*, *40*(1), 27–67, doi:10.1080/02786820500421521.

Braun, A., F. E. Huggins, N. Shah, Y. Chen, S. Wirick, S. B. Mun, C. Jacobsen, and G. P. Huffman (2005), Advantages of soft X-ray absorption over TEM-EELS for solid carbon studies—A comparative study on diesel soot with EELS and NEXAFS, *Carbon*, *43*, 117–124, doi:10.1016/j.carbon.2004.08.029.

Buseck, P. R., and M. Pósfai (1999), Airborne minerals and related aerosol particles: Effects on climate and the environment, *Proc. Natl. Acad. Sci. U. S. A.*, *96*(7), 3372–3379, doi:10.1073/pnas.96.7.3372.

Buseck, P. R., H. Bo-Jun, and L. P. Keller (1987), Electron microscope investigation of the structure of annealed carbons, *Energy Fuels*, *1*, 105–110, doi:10.1021/ef00001a020.

Chen, Y. Z., N. Shah, A. Braun, F. E. Huggins, and G. P. Huffman (2005), Electron microscopy investigation of carbonaceous particulate matter generated by combustion of fossil fuels, *Energy Fuels*, *19*, 1644–1651, doi:10.1021/ef049736y.

Choël, M., K. Deboudt, J. Osán, P. Flament, and R. Van Grieken (2005), Quantitative determination of low-Z elements in single atmospheric particles on boron substrates by automated scanning electron microscopy-energy-dispersive X-ray spectrometry, *Anal. Chem.*, *77*, 5686–5692, doi:10.1021/ac050739x.

Choël, M., K. Deboudt, and P. Flament (2007), Evaluation of quantitative procedures for X-ray microanalysis of environmental particles, *Microsc. Res. Tech.*, *70*(11), 996–1002, doi:10.1002/jemt.20510.

Choël, M., K. Deboudt, and P. Flament (2010), Development of time-resolved description of aerosol properties at the particle scale during an episode of industrial pollution plume, *Water Air Soil Pollut.*, *209*, 93–107, doi:10.1007/s11270-009-0183-9.

Chou, C., P. Formenti, M. Maille, P. Ausset, G. Helas, M. Harrison, and S. Osborne (2008), Size distribution, shape, and composition of mineral dust aerosols collected during the African Monsoon Multidisciplinary Analysis Special Observation Period 0: Dust and Biomass-Burning Experiment field campaign in Niger, January 2006, *J. Geophys. Res.*, *113*, D00C10, doi:10.1029/2008JD009897.

Derimian, Y., J. F. Leon, O. Dubovik, I. Chiapello, D. Tanre, A. Sinyuk, F. Auriol, T. Podvin, G. Brogniez, and B. N. Holben (2008), Radiative properties of aerosol mixture observed during the dry season 2006 over M'Bour, Senegal (African Monsoon Multidisciplinary Analysis campaign), *J. Geophys. Res.*, *113*, D00C09, doi:10.1029/2008JD009904.

Draxler, R. R., and G. D. Hess (1998), An overview of the Hysplit_4 Modeling System for Trajectories, Dispersion, and Deposition, *Aust. Meteorol. Mag.*, *47*(4), 295–308.

Ebert, M., S. Weinbruch, P. Hoffmann, and H. M. Ortner (2004), The chemical composition and complex refractive index of rural and urban influenced aerosols determined by individual particle analysis, *Atmos. Environ.*, *38*, 6531–6545, doi:10.1016/j.atmosenv.2004.08.048.

Echalar, F., A. Gaudichet, H. Cachier, and P. Artaxo (1995), Aerosol emissions by tropical forest and savanna biomass burning: Characteristic trace elements and fluxes, *Geophys. Res. Lett.*, *22*, 3039–3042, doi:10.1029/95GL03170.

Falkovich, A. H., G. Schkolnik, E. Ganor, and Y. Rudich (2004), Adsorption of organic compounds pertinent to urban environments onto mineral dust particles, *J. Geophys. Res.*, *109*, D02208, doi:10.1029/2003JD003919.

Finlayson-Pitts, B. J., and J. N. J. Pitts (2000), *Chemistry of the Upper and Lower Atmosphere—Theory, Experiments and Applications*, 969 pp., Academic, San Diego, Calif.

Formenti, P., W. Elbert, W. Maenhaut, J. Haywood, and M. O. Andreae (2003), Chemical composition of mineral dust aerosol during the Saharan Dust Experiment (SHADE) airborne campaign in the Cape Verde region, September 2000, *J. Geophys. Res.*, *108*(D18), 8576, doi:10.1029/2002JD002648.

Gao, Y., L. E. Yu, and S. B. Chen (2008), Effects of organics on efflorescence relative humidity of ammonium sulfate or sodium chloride particles, *Atmos. Environ.*, *42*, 4433–4445, doi:10.1016/j.atmosenv.2008.02.002.

Gloter, A., A. Douiri, M. Tence, and C. Colliex (2003), Improving energy resolution of EELS spectra: An alternative to the monochromator solution, *Ultramicroscopy*, *96*, 385–400, doi:10.1016/S0304-3991(03)00103-7.

Hand, J. L., et al. (2005), Optical, physical, and chemical properties of tar balls observed during the Yosemite Aerosol Characterization Study, *J. Geophys. Res.*, *110*, D21210, doi:10.1029/2004JD005728.

Hansen, A. D. A. (2003), *The Aethalometer Manual*, Magee Scientific, Berkeley, Calif.

Haywood, J. M., et al. (2008), Overview of the Dust and Biomass-burning Experiment and African Monsoon Multidisciplinary Analysis Special Observing Period-0, *J. Geophys. Res.*, *113*, D00C17, doi:10.1029/2008JD010077.

Hobert, H. (1995), Characterization of atmospheric dust sediments by using infrared spectroscopy: Dust spectra and an analytical model, *Vib. Spectrosc.*, *9*, 169–179, doi:10.1016/0924-2031(94)00085-U.

Hopkins, R. J., A. V. Tivanski, B. D. Marten, and M. K. Gilles (2007), Chemical bonding and structure of black carbon reference materials and individual carbonaceous atmospheric aerosols, *J. Aerosol Sci.*, *38*, 573–591, doi:10.1016/j.jaerosci.2007.03.009.

Hopkins, J. R., M. J. Evans, J. D. Lee, A. C. Lewis, J. H. Marsham, J. B. McQuaid, D. J. Parker, D. J. Stewart, C. E. Reeves, and R. M. Purvis (2009), Direct estimates of emissions from the megacity of Lagos, *Atmos. Chem. Phys.*, *9*, 8471–8477, doi:10.5194/acp-9-8471-2009.

Ivleva, N. P., U. McKeon, R. Niessner, and U. Poschl (2007), Raman microspectroscopic analysis of size-resolved atmospheric aerosol particle samples collected with an ELPI: Soot, humic-like substances, and inorganic compounds, *Aerosol Sci. Technol.*, *41*(7), 655–671, doi:10.1080/02786820701376391.

Jacobson, M. Z. (2001), Strong radiative heating due to the mixing state of black carbon in atmospheric aerosols, *Nature*, *409*, 695–697, doi:10.1038/35055518.

Johnson, B. T., S. R. Osborne, J. M. Haywood, and M. A. J. Harrison (2008), Aircraft measurements of biomass burning aerosol over West Africa during DABEX, *J. Geophys. Res.*, *113*, D00C06, doi:10.1029/2007JD009451.

Katrinak, K. A., P. Rez, and P. R. Buseck (1992), Structural variations in individual carbonaceous particles from an urban aerosol, *Environ. Sci. Technol.*, *26*, 1967–1976, doi:10.1021/es00034a014.

Kirchstetter, T. W., T. Novakov, and P. V. Hobbs (2004), Evidence that the spectral dependence of light absorption by aerosols is affected by organic carbon, *J. Geophys. Res.*, *109*, D21208, doi:10.1029/2004JD004999.

Laskin, A., and J. P. Cowin (2001), Automated single-particle SEM/EDX analysis of submicrometer particles down to 0.1 μm, *Anal. Chem.*, *73*, 1023–1029, doi:10.1021/ac0009604.

Leaitch, W. R., et al. (2009), Evidence for Asian dust effects from aerosol plume measurements during INTEX-B 2006 near Whistler, BC, *Atmos. Chem. Phys.*, *9*, 3523–3546, doi:10.5194/acp-9-3523-2009.

Lee, S.-H., D. M. Murphy, D. S. Thomson, and A. M. Middlebrook (2002), Chemical components of single particles measured with Particle Analysis by Laser Mass Spectrometry (PALMS) during the Atlanta SuperSite Project: Focus on organic/sulfate, lead, soot, and mineral particles, *J. Geophys. Res.*, *107*(D1), 4003, doi:10.1029/2000JD000011.

Liousse, C., J. E. Penner, C. Chuang, J. J. Walton, H. Eddleman, and H. Cachier (1996), A global three-dimensional model study of carbonaceous aerosols, *J. Geophys. Res.*, *101*(D14), 19,411–19,432, doi:10.1029/95JD03426.

Liu, X. D., P. Van Espen, F. Adams, J. Cafmeyer, and W. Maenhaut (2000), Biomass burning in southern Africa: Individual particle characterization of atmospheric aerosols and savanna fire samples, *J. Atmos. Chem.*, *36*, 135–155, doi:10.1023/A:1006387031927.

Ma, C.-J., S. Tohno, M. Kasahara, and S. Hayakawa (2004), Properties of individual Asian dust storm particles collected at Kosan, Korea during ACE-Asia, *Atmos. Environ.*, *38*, 1133–1143, doi:10.1016/j.atmosenv.2003.11.020.

Mavrocordatos, D., W. Pronk, and M. Boller (2004), Analysis of environmental particles by atomic force microscopy, scanning and transmission electron microscopy, *Water Sci. Technol.*, *50*(12), 9–18.

Osborne, S. R., B. T. Johnson, J. M. Haywood, A. J. Baran, M. A. J. Harrison, and C. L. McConnell (2008), Physical and optical properties of mineral dust aerosol during the Dust and Biomass-burning Experiment, *J. Geophys. Res.*, *113*, D00C03, doi:10.1029/2007JD009551.

Pósfai, M., H. Xu, J. R. Anderson, and P. R. Buseck (1998), Wet and dry sizes of atmospheric aerosol particles: An AFM-TEM study, *Geophys. Res. Lett.*, *25*, 1907–1910, doi:10.1029/98GL01416.

Pósfai, M., R. Simonics, J. Li, P. V. Hobbs, and P. R. Buseck (2003), Individual aerosol particles from biomass burning in southern Africa: 1. Compositions and size distributions of carbonaceous particles, *J. Geophys. Res.*, *108*(D13), 8483, doi:10.1029/2002JD002291.

Pósfai, M., A. Gelencser, R. Simonics, K. Arato, J. Li, P. V. Hobbs, and P. R. Buseck (2004), Atmospheric tar balls: Particles from biomass and biofuel burning, *J. Geophys. Res.*, *109*, D06213, doi:10.1029/2003JD004169.

Rajot, J. L., et al. (2008), AMMA dust experiment: An overview of measurements performed during the dry season special observation period (SOP0) at the Banizoumbou (Niger) supersite, *J. Geophys. Res.*, *113*, D00C14, doi:10.1029/2008JD009906.

Ro, C.-U., J. Osán, I. Szalóki, J. de Hoog, A. Worobiec, and R. Van Grieken (2003), A Monte Carlo program for quantitative electron-induced X-ray analysis of individual particles, *Anal. Chem.*, *75*, 851–859, doi:10.1021/ac025973r.

Ro, C.-U., H. Hwang, H. Kim, Y. Chun, and R. Van Grieken (2005), Single-particle characterization of four "Asian dust" samples collected in Korea, using low-Z particle electron probe X-ray microanalysis, *Environ. Sci. Technol.*, *39*, 1409–1419, doi:10.1021/es049772b.

Roessler, D. M., F. R. Faxvog, R. Stevenson, and G. W. Smith (1981), Optical properties and morphology of particulate carbon: Variation with air/fuel ratio, in *Particulate Carbon: Formation During Combustion*, edited by D. C. Siegla and G. W. Smith, pp. 57–89, Plenum, New York.

Russell, L. M., S. F. Maria, and S. C. B. Myneni (2002), Mapping organic coatings on atmospheric particles, *Geophys. Res. Lett.*, *29*(16), 1779, doi:10.1029/2002GL014874.

Sadezky, A., H. Muckenhuber, H. Grothe, R. Niessner, and U. Pöschl (2005), Raman microspectroscopy of soot and related carbonaceous materials: Spectral analysis and structural information, *Carbon*, *43*, 1731–1742, doi:10.1016/j.carbon.2005.02.018.

Seinfeld, J. H., and S. N. Pandis (1998), *Atmospheric Chemistry and Physics: From Air Pollution to Climate Change*, John Wiley, New York.

Stunder, B. J. B. (1997) NCEP model output, *Tech. Rep. TD-6141*, NOAA Air Resour. Lab., Silver Spring, Md.

Sullivan, R. C., and K. A. Prather (2007), Investigations of the diurnalcycle and mixing state of oxalic acid in individual particles in Asian aerosol outflow, *Environ. Sci. Technol.*, *41*, 8062–8069, doi:10.1021/es071134g.

Sullivan, R. C., S. A. Guazzotti, D. A. Sodeman, and K. A. Prather (2007), Direct observations of the atmospheric processing of Asian mineral dust, *Atmos. Chem. Phys.*, *7*, 1213–1236, doi:10.5194/acp-7-1213-2007.

Takahama, S., S. Liu, and L. M. Russell (2010), Coatings and clusters of carboxylic acids in carbon-containing atmospheric particles from spectromicroscopy and their implications for cloud-nucleating and optical properties, *J. Geophys. Res.*, *115*, D01202, doi:10.1029/2009JD012622.

Tuinstra, F., and J. L. Koenig (1970), Raman spectrum of graphite, *J. Chem. Phys.*, *53*, 1126–1130, doi:10.1063/1.1674108.

Usher, C. R., A. E. Michel, and V. H. Grassian (2003), Reactions on mineral dust, *Chem. Rev.*, *103*(12), 4883–4940, doi:10.1021/cr020657y.

van Vliet, E. D. S., and P. L. Kinney (2007), Impacts of roadway emissions on urban particulate matter concentrations in sub-Saharan Africa: New evidence from Nairobi, *Environ. Res. Lett.*, *2*, 045028, doi:10.1088/1748-9326/2/4/045028.

Wentzel, M., H. Gorzawski, K. H. Naumann, H. Saathoff, and S. Weinbruch (2003), Transmission electron microscopical and aerosol dynamical characterization of soot aerosols, *J. Aerosol Sci.*, *34*, 1347–1370, doi:10.1016/S0021-8502(03)00360-4.

Worobiec, A., I. Szalóki, J. Osán, W. Maenhaut, E. Anna Stefaniak, and R. Van Grieken (2007), Characterisation of Amazon Basin aerosols at the individual particle level by X-ray microanalytical techniques, *Atmos. Environ.*, *41*, 9217–9230, doi:10.1016/j.atmosenv.2007.07.056.

M. Choël, K. Deboudt, P. Flament, and S. Sobanska, Université Lille Nord de France, F-59000 Lille, France. (karine.deboudt@univ-littoral.fr)

C. Colliex and A. Gloter, Laboratoire de Physique des Solides, UMR CNRS 8502, Université de Paris-Sud 11, CNRS, F-91405 Orsay, France.